ROYAL SOCIETY OF CHEMISTRY

PAPER

Check for updates

Unique calibration of passive air sampling for field monitoring of PAHs with polyethylene thin films across seasons and locations†

Jana Meierdierks, [iD] *[a] Christiane Zarfl,[a] Barbara Beckingham [iD] [b] and Peter Grathwohl[a]

Although passive sampling has been applied to determine concentrations of semi-volatile organic chemicals such as polycyclic aromatic hydrocarbons (PAHs) in air and water for about two decades and is well established, several uncertainties and challenges remain. This study presents a comprehensive validation of polyethylene thin sheets as passive air samplers (PE-PAS), detailing alternative approaches to calibration and analysis. Besides measuring the uptake kinetics in the field using time series deployments of PE-PAS at 3 field sites under varying seasonal conditions (temperature, wind) with a performance reference compound (PRC), we implement a numerical model to fit uptake kinetics based on partition and diffusion coefficients adapted to hourly changes of temperature. This model follows similar approaches as reported in earlier studies, but we use loss curves of a spiked PRC (anthracene-D_{10}) to fit the air-side boundary layer (δ_g), which is limiting mass transfer between air and PE, instead of calibrating the PAS sampling rate. Surprisingly, air side boundary layers, and thus inherent sampling rates, were almost equal at the different locations but varied for the different sampling campaigns by about a factor of two. This variation is probably due to short term effects, but a robust average over all seasons and locations could be obtained (1 mm ± 0.5 mm) which is characteristic for our sampling design. A well-known δ_g allows concentrations in air of compounds with very different uptake kinetics onto the PE-PAS to be estimated. Additionally, as in previous studies, our results indicate stable distribution patterns of PAHs in the environment of the study region in Germany. Given a practical chosen PE-PAS deployment time, representative compounds may be selected that integrate over the desired monitoring time period (*e.g.* fluorene for days, phenanthrene for weeks and pyrene or fluoranthene for many months to years). Measurement of one PAH applied with specific ratios derived from stable distribution patterns of PAHs, in the absence of influential local point sources, can then be used to estimate air concentrations of PAHs that are more difficult to quantify during the monitoring period.

Environmental significance

The investigation of Polycyclic Aromatic Hydrocarbons (PAHs) in air in general is environmentally relevant, since (i) PAHs are characterized as a class of contaminants with special concern due to their toxic behaviour and relatively long persistence and (ii) both emission and transport with subsequent distribution of these compounds in the environment mainly occur in the air. In our study we provide a method to determine PAH concentrations in air that can be easily, reproducibly and reliably applied. Thus, we aim for an improvement of the widely used passive air sampling of PAHs.

1. Introduction

Determining atmospheric concentrations of the broad range of chemicals being introduced into the environment is important because many chemicals show extreme persistence and potential for long-range transport, reaching even remote areas, and monitoring can improve our understanding of environmental fate, human and environmental health risks, and regulatory actions.[1–3] Application of passive samplers has increased remarkably during the last years to detect contaminants in various environmental media,[4–6] including in air as reviewed by Wania & Shunthirasingham.[7] Passive sampling applications are diverse and include the study of contaminant spatial and temporal distribution over various scales as well as to determine cross-compartment fugacity gradients that enable observation

[a] Center for Applied Geosciences, University of Tübingen, Schnarrenbergstraße 94-96, 72076 Tübingen, Germany. E-mail: jana.meierdierks@uni-tuebingen.de

[b] Department of Geology and Environmental Geosciences, College of Charleston, Charleston, SC, USA

† Electronic supplementary information (ESI) available. See DOI: 10.1039/d0ea00022a

© 2021 The Author(s). Published by the Royal Society of Chemistry

Environ. Sci.: Atmos., 2021, **1**, 253–266 | **253**

of fluxes.[8–13] In particular, in remote areas and for long-term sampling campaigns, passive air sampling (PAS) gets more attractive than active air sampling due to high effort for maintenance and energy supply.[14] Application of PAS thus far is mainly semi-quantitative[15] or used to examine prevailing flux direction rather than fluctuation in rates[16,17] and still several uncertainties exist.[7]

The theory of passive sampling is well described in literature.[4,18–22] Following a double-film diffusion conceptual model,[23] equilibrium conditions exist at the interface of a PAS and air, with concentration gradients evolving on both sides leading to boundary layers at the air-side (δ_g) and the sampler-side (δ_p) which act as mass transfer resistances.[21] Because of relatively high partitioning coefficients (K_{pg}), it is widely accepted that the air-side boundary layer is controlling the uptake process of semi- and low volatile atmospheric compounds onto various polymer passive samplers depending on deployment set-up.[4,19,22,24] Uptake onto the passive sampler occurs in three phases: kinetic (linear), intermediate (curvilinear) and dynamic equilibrium (plateau).[4,25] For the translation of measured concentrations on passive air samplers into gas concentrations in the atmosphere, the sampled uptake phase of the target compounds needs consideration; if the uptake of target compounds onto passive air samplers exceeds the linear phase but does not yet reach equilibrium between air and sampler, information on both the uptake kinetics and equilibrium (*i.e.* the partition coefficient) needs to be known.[25,26] Both the exchange kinetics and the partition coefficient are influenced by environmental conditions; K_{pg} varies with temperature, while the kinetics are additionally influenced by the wind speed. For instance, high wind speeds result in thinner boundary layers and thus in faster kinetics meaning higher sampling rates and shorter equilibration time scales.[27,28]

Calibrating passive sampling kinetics in the lab or additionally using active samplers in the field is a commonly used approach but cannot account for varying atmospheric conditions.[28–30] Therefore, often several performance reference compounds (PRCs) are used for *in situ* calibration of passive samplers.[27,31,32] Based on the measured loss of PRCs the uptake of target compounds on PAS is calibrated with mathematical models (see below). Although PRC loss is a widely applied method for calibrating exchange kinetics in passive sampling, few studies focus on a quantification of the air-side boundary layer parameter.

Polycyclic aromatic hydrocarbons (PAHs) are a class of contaminants of concern due to being potential human carcinogens as well as exerting other toxicities, and having relatively long half-lives. They typically occur in much higher concentration in soils, sediments and the atmosphere than other persistent organic compounds. Anthropogenic emission of PAHs is mainly caused by the incomplete combustion of fuels, so typical emission sources are industrial processes, biomass/waste combustion, domestic heating and traffic.[33–36] PAHs occur as mixtures and their physico-chemical properties range over orders of magnitude, which poses a challenge for environmental sampling. PAHs may undergo long range transport, they are stored and re-volatilized from terrestrial compartments[37–39] and surface seawater[12,40] and re-enter the atmosphere. Diffuse sources and mixing processes lead to rather stable distribution patterns of PAHs in air which may remain relatively constant in time and space for a region without strong influence of specific primary sources. Such stable characteristic ratios of individual PAHs sensed by PAS might be applied as a new approach to extrapolating measured concentrations of less volatile target compounds that require longer integration times to be detected on the sampler. This should enable concentration estimates for compounds that are routinely difficult to measure and quantify.

The objectives of this study were to (i) gain understanding of the kinetics and time scales for passive sampling of PAHs in air with PE thin sheets under field conditions in different seasons, (ii) determine air-side boundary layer thicknesses using numerical models to calculate concentrations of PAHs in air, and (iii) analyse the suitability of PAH distribution patterns to reduce actual pollutant measurements to one indicator PAH. Fluorene (Fln), phenanthrene (Phe), fluoranthene (Fth) and pyrene (Pyr) were chosen as representative PAHs within this study based on their partition coefficients (PE-air), as they cover a broad range of almost two log units (Table 1), and because they are commonly detected at relatively high concentrations on the sampler and thus offer reliability and lower uncertainty for measurements. Pyr is the only high molecular weight PAH which could be detected in sufficiently high concentrations during all monitoring periods. Anthracene-D10 (Ant-D_{10}) was used as a performance reference compound for the planned deployments since it shows a significant release (>50%) from the sampler within a few days. Ant-D_{10} does not occur in the atmosphere and has similar physicochemical properties as

Table 1 Properties of fluorene (Fln), phenanthrene (Phe), fluoranthene (Fth) and pyrene (Pyr) (representative PAHs) and anthracene-D10 (Ant-D_{10}) used as performance reference compound: molar volume (V_m), molecular weight (MW), diffusion coefficient in PE (p), diffusion coefficient in gas phase (D_g), polyethylene/gas phase partition coefficient (K_{pg} at 25 °C) and enthalpy of vaporization (ΔH_{vap})

Compound	V_m [cm^3 mol^{-1}]	MW [g mol^{-1}]	log $D_p{}^a$ [m^2 s^{-1}]	log D_g [m^2 s^{-1}]	log $K_{pg}{}^{ac}$ [L kg^{-1}]	$\Delta H_{vap}{}^b$ [kJ mol^{-1}]
FLN	193.9	166.22	−12.36	−5.23	6.3	72.1
Ant-D_{10}	190.2	178.23	−12.44	−5.22	7.1	79.9
PHE	190.2	178.23	−12.44	−5.22	7.0	78.3
FTH	223.2	202.25	−12.96	−5.26	8.1	87.1
PYR	203	202.25	−12.76	−5.24	8.1	89.4

^{a} Lohmann.[42] ^{b} Roux, Temprado.[36] ^{c} K_{pg} has uncertainties of approx. 0.4 log units for the different approaches to determine this value.[20,42,43]

254 | *Environ. Sci.: Atmos.*, 2021, **1**, 253–266

© 2021 The Author(s). Published by the Royal Society of Chemistry

phenanthrene, the most abundant PAH. We chose to study PE thin sheets because of their relative low cost, simplicity in handling in the field and the lab, and demonstrated promise for use as a PAS in previous studies.[22,41] However, use of PE sheets may have disadvantages derived from its relatively low capacity in comparison to infinite sink samplers, which complicates the data evaluation in terms of the uptake phase of different compounds and their integration time span.

2. Materials and methods

2.1. Air sampling

Materials. Commercial low-density polyethylene (LDPE, or short: PE) sheets of 80 μm thickness were used as passive samplers (JUFOL GmbH). All solvents used for extraction had a certified purity of 99.8% and were supplied by Merck Millipore (Darmstadt, Germany). Ultrapure water was obtained by a water purification system (Gen Pure Pro UV-TOC, Thermo Scientific). The external (PAH Mix 14, Dr Ehrenstorfer GmbH) and internal standards (PAH Mix 31, Dr Ehrenstorfer GmbH) had a certified purity of >98%, and both were used for quantification of the target compounds. The deuterated anthracene (Ant-D_{10}, Dr Ehrenstorfer GmbH) had a certified purity of 99.0%.

Preparation of the PE passive samplers. Sheets of PE thin film were cut into strips of 9 × 25 cm and perforated at two spots to allow easy and fast deployment on hangers in the field. For precleaning, PE was shaken for 24 h in cyclohexane followed by 24 h in ethylacetate followed by several rinsing steps with ultrapure water. In advance of the deployment, samplers were spiked with deuterated anthracene (Ant-D_{10}) as PRC using a procedure adapted from Booij.[44] In brief, PE was placed in a spiked solution of ultrapure-water : methanol (80 : 20% vol) with masses optimized to achieve a desired Ant-D_{10} starting concentration and mixed for seven days on an overhead shaker. The prepared PE-PAS were taken out of the spiking solution, wiped dry of solution and wrapped thoroughly in aluminium foil right before transportation into the field.

Deployment, sampling and extraction. Three study sites (Entringen, Poltringen, Tailfingen – see Fig. S1†) in the hinterland of Stuttgart in southwestern Germany were chosen for regular monitoring campaigns. All sites were formerly or recently used for agriculture and local point sources of PAHs could be mostly excluded. In the field, PE-PAS were deployed within an open-bottomed aluminium box cover at 1.2 m height to reduce exposure to wind, direct sunlight and dust (Fig. S2†). Samplers ($N = 21$) were placed in two rows within one box with 4.5 cm distance between them. Sampling campaigns were initiated on 3-May 2016, 1-August 2016, 1-November 2016, 3-February 2017, 1-May 2017, 1-August 2017, 3-November 2017 and 1-February 2018. At the beginning of each sampling campaign, samples were taken in a high resolution (12, 24, 48, 72, 120 hours), followed by 10, 20 and 30 days (and 36 days for February 2017) to monitor the uptake kinetics of the target compounds and the loss of the PRC (during the second year of sampling, the sampling resolution varied slightly with an additional sampling after 15 days). At sampling, the PE was rinsed with ultrapure water and wiped dry with lint-free tissue

to remove potential particles. For the extraction, PE was shaken with 50 mL of ethylacetate twice for 24 hours. Internal standard (PAH-Mix 31 deuterated, Dr Ehrenstorfer GmbH) was added to the combined extracts before reducing the volume to 10 mL using a rotational evaporator (at 40 °C and 215 mbar). In preliminary analyses we observed the clearest chromatograms, without superimposing peaks, when extracts were mixed with 800 mL ultrapure water before solvent exchange with an addition of 10 mL of cyclohexane shaken for 30 minutes. Subsequently, the solvent phase was transferred into clean vials, heated to 40 °C and reduced under a gentle nitrogen stream to 200 μL.

Active sampling. Active sampling was performed over 3–5 days periods twice during November–December 2017 and twice during February 2018, aiming to sample about 4 m³ of air each time to provide enough gaseous PAHs for reliable quantification. Due to logistical reasons, active sampling was done in triplicates in Entringen instead of at each site. Personal air sampling pumps (Gilian 5000) were set at a flow rate of 1 L min^{-1}, which was calibrated using a flow-through-meter (Rotameter, Fisher Bioblock). Since there was no power supply at the sampling site, pumps were brought into the lab every 16 hours for battery-recharge, and thus stopped regularly for intervals of up to 8 hours. Cartridges (2.5 cm in diameter) containing one glass fibre filter (GFF) (0.45 μm, Whatman) and two subsequent polyurethane foam (PUF) filters of 1 cm thickness each (TISCH Environmental) were used. Before deployment, the PUF filters were cleaned by Soxhlet extraction with acetone for 12 hours. After the sampling, all glass fibre and polyurethane filters were extracted separately with an Accelerated Solvent Extractor (ASE) using ethylacetate as solvent at 85 °C during 3, 20 min extraction cycles. Internal standard was added into the extracts before shaking with ultrapure water and transferring into cyclohexane in the process described above.

Quality control and uncertainty. Several types of material controls were performed to check for background contamination. Precleaned, PRC-spiked PE-PAS were analyzed by extracting samplers in triplicate at the time of preparation. Additionally, to determine potential contamination during transport, triplicate field blanks taken to each field site on the day of deployment set-up were analyzed. Blank PUF filters were extracted to assess the potential for lab contamination right after the clean-up, and GFF as well as PUF field blanks were sampled from cartridges that were not attached to pumps but otherwise handled the same as the samples taken to field sites. Concentrations measured on PE-PAS, GFF and PUF during the monitoring period were corrected by the respective lab and field blanks.

Measurement uncertainties that propagate in the model were considered. Internal and external standard variation may affect target analyte quantitation by up to 10%. Manual integration of peak areas introduces another uncertainty, which gets most pronounced for small peaks and can reach up to 20%. Based on those observations, the confidence interval for comparing different sets of concentrations was generally set to ±30%. The relative standard deviation of the replicate samples was generally below 15%, with some exceptions for small

© 2021 The Author(s). Published by the Royal Society of Chemistry

Environ. Sci.: Atmos., 2021, **1**, 253–266 | **255**

concentrations. As expected, the standard deviation increased when combining the three locations, which was again most significant for low concentrations and high temperatures.

2.2. Analysis and evaluation

Measurement. Concentrations of the target compounds were determined by gas chromatography with coupled mass spectrometry (Hewlett Packard [HP] 68909 and HP 5973) using a 25 m long capillary column (25 μm inner diameter, 0.25 μm thick film of 5% phenyl- and 95% dimethyl-polysiloxane; J&W Scientific). Samples were injected in pulsed splitless mode. The temperature program started with an initial temperature of 65 °C for 4 minutes, with temperature ramped 10 °C min^{-1} to 270 °C, held constant for 10 minutes, and then ramped again at the same rate to 310 °C and held for 6 minutes. Helium was used as inert carrier gas with a constant flow rate of 0.7 mL min^{-1}. The mass spectrometer was operated in selected ion monitoring mode.

Mathematical models and data evaluation. Our data evaluation follows the common approach of a first order exponential equation to describe the exchange kinetics between sampler (PE) and sampled medium (air).[12,19,31,45] The loss of PRCs over time is defined by the loss rate constant k_e [s^{-1}] and can be described as:

$$C_{PRC,t} = C_{PRC,t}e^{(-k_e t)} \quad (1.1)$$

$C_{PRC,t}$ [ng g^{-1}] denotes the concentration of the PRC on the passive sampler at time t [s] and $C_{PRC,0}$ [ng g^{-1}] is the initial concentration. k_e is obtained by fitting the slope of the release curves of the PRC[15,31,42] and depends on the partition coefficient (PE-air), the geometry of the passive sampler as well as on mass transfer, i.e. diffusion through the air side boundary layer which is limiting for thin sheets and compounds with $K_{OA} > 10^6$,[46] as observed in earlier studies.[47] The loss rate constant for the PRC is:

$$k_e = \frac{2D_{g-PRC}}{d_p K_{pg-PRC}\rho_p\delta_g} \quad (1.2)$$

where D_{g-PRC}, K_{pg-PCR}, ρ_p and d_p denote the diffusion coefficient in gas phase [m^2 s^{-1}] and the partition coefficient between sampler and air [L kg^{-1}] of the PRC, and the density [kg L^{-1}] and the thickness of the passive sampler [m], respectively. $2/d_p$ represents the specific surface area of a thin sheet [m^2 m^{-3}]. This approach is equivalent to earlier studies, which use the inherent sampling rates (RS) of passive samplers as RS = $D_g/\delta_g A_s$ (with A_s as the surface area of the samplers). The difference in our approach is that we account for the area and D_g separately. For compounds with similar diffusivities, the air-side boundary layer is independent of the target compound and can be determined from k_e of the PRC:

$$\delta_g = \frac{2D_{g-PRC}}{d_p K_{pg-PRC}\rho_p k_e} \quad (1.3)$$

If δ_g is known, individual uptake rate constants (k_{up} [s^{-1}]) can be calculated using 1.2 but for diffusion and partitioning coefficients for each target compound, assuming a stable δ_g in the

sampling period. Uptake of the target compounds onto the passive sampler is:

$$\frac{C_{p,t\text{-target}}}{C_{p,eq}} = 1 - e^{(-\lambda k_{up}t)} \quad (1.4)$$

Atmospheric concentrations can also be calculated with the analytical solution,[12,13,31] adapting eqn (1.4) accordingly to:

$$C_{g\text{-target}} = \frac{C_{p,t\text{-target}}}{[1 - \exp(-k_{up}t)]K_{pg\text{-target}}} \quad (1.5)$$

Note that for early times the argument of the exponential function is very small and may be used directly $(1 - \exp(-x) = x)$; thus, in this early stage the uptake of a compound is linear and becomes independent on the partitioning of the compound or the temperature (K_{pg} drops out).

The rate constant allows comparison of the sampled time spans for the individual compounds since the characteristic times to reach 63% equilibrium may be estimated as the inverse of the respective rate constant:

$$t_{0.63} = \frac{1}{k_e} \quad \text{or} \quad = \frac{1}{k_{up}} \text{ for the PRC and the target compound} \quad (1.6)$$

This characteristic time is chosen for convenience of calculation and does not represent a specific uptake phase. Since gaseous diffusion coefficients of PAHs are similar, the time scales over which a passive sampler integrates consequently increases with increasing K_{pg} (1.2). Thus, linear and curvilinear uptake phases (and $t_{0.63}$) occur at very different time scales for different compounds, which is a major difficulty for PAS sampling using thin PE sheets.[7] Since partition coefficients between PE and gas phase of the 16 U.S. EPA priority PAHs cover a range of more than four orders of magnitude,[42] high molecular weight PAHs equilibrate 10 000 times slower than low molecular weight compounds. K_{pg} depends on temperature (to some minor extent this also applies to D_g), which may be different in each time interval; additionally, the exchange kinetics are influenced by wind speed,[28,30] although this is reduced by the wind-protected sampling design and is accounted for by calibrating δ_g.

To account for the temperature-dependent varying values of K_{pg} and D_g, Fick's first law can be solved numerically using the differential equation for uptake of a compound from the gas phase:

$$\frac{dC_p}{dt} = -\frac{D_g}{\delta_g}\frac{2}{d_p\rho_p}\left(\frac{C_p}{K_{pg}} - C_g\right) \quad (1.7)$$

Solving this equation step-wise provides discrete C_p values after each time step (dt):

$$C_{p,t+1} = \left[-\frac{D_{g,t}}{\delta_g}\frac{2}{d_p\rho_p}\left(\frac{C_{p,t}}{K_{pg}} - C_g\right)\right]dt + C_{p,t} \quad (1.8)$$

© 2021 The Author(s). Published by the Royal Society of Chemistry

C_p/K_{pg} denotes the gas phase concentration at the polymer/air interface which allows to calculate the concentration difference across the air-side boundary layer. D_g/δ_g is the mass transfer coefficient [m s^{-1}]. K_{pg} and D_g can be adjusted for each time step according to temperature conditions. Partition coefficients can be calculated for different temperatures (T_1 and T_2 in kelvin) following the van't Hoff equation and using the enthalpy of vaporization, according to Khairy and Lohmann:[22,48]

$$K_{pg(T_2)} = K_{pg(T_1)} \exp\left[\frac{\Delta H_{vap}}{R}\left(\frac{1}{T_2} - \frac{1}{T_1}\right)\right] \quad (1.9)$$

$K_{pg(T_1)}$ is the partitioning coefficient at standard temperature T_1 (*e.g.* 298.15 K, here taken from Khairy and Lohmann[22]) and R denotes the ideal gas constant (8.314 × 10^{-3} kJ (mol^{-1} K^{-1})). The evaporation enthalpy ΔH_{vap} is typically ~80 kJ mol^{-1} (see Table 1) and thus a decrease of temperature by 20 °C would cause an increase of K_{pg} by a factor of 10. The diffusion coefficient in the gas phase D_g (in [m^2 s^{-1}]) can be calculated for the respective temperature following the Fuller–Schettler–Giddings-method:

$$D_g = \frac{10^{-3} T^{1.75}\sqrt{M_{PAH}^{-1} + M_g^{-1}}}{P\left(V_{PAH}^{1/3} + V_g^{1/3}\right)} \quad (1.10)$$

M_{PAH}, M_g, V_{PAH}, V_g, P denote molecular mass [g mol^{-1}] of the compound of interest and of air, their molar volumes [m^3 mol^{-1}] and atmospheric pressure [atm].

During PRC loss, the air side boundary layer thickness δ_g is the only unknown parameter in our setup (see eqn (1.7)). In a first step, the numerical model was applied to calibrate this air-side boundary layer as a constant value for each sampling campaign by location. A Gauß–Newton type least-square method implemented in the optimization toolbox of Matlab (lsqcurvefit) was utilized to correlate the calculated concentrations on the PE to the measured data set by fitting δ_g. Diffusion and partition coefficients were adapted to the current temperatures during each sampling period based on hourly measurements, provided by the German Weather Survey, measured at the close-by airport in Stuttgart-Echterdingen (48.6915°, 9.1939°). A residual concentration of Ant-D$_{10}$ (*ca.* 5% of the initial spiking) on PE-PAS remained even after several weeks in the field, which was considered in the fitting routine calculating δ_g, but did not influence the resulting δ_g. For comparison, δ_g was also fitted to the uptake of Phe onto the sampler. Since concentrations on PE were very similar for the three sites, data were merged to obtain one average δ_g for each monitoring, which is discussed in Section 3.3. Phenanthrene was chosen since its physicochemical properties are almost the same as for Ant, the linear uptake phase of Phe onto PE is long enough to be sampled, and Phe reaches equilibrium on the sampler during each monitoring. At equilibrium, the atmospheric concentrations of Phe can be determined simply by using the equilibrium partition coefficient ($C_{g,eq} = C_{p,eq}/K_{pg}$) and δ_g remains as the only unknown fitting parameter.

For the other target compounds, a fixed air-side boundary layer thickness was implemented into the numerical model (eqn (1.7)) and C_g remains as the only unknown parameter, which was fitted with the same fitting routine as applied for δ_g. As in other approaches, C_g is assumed to be stable during the monitoring, as our model fits only one (average) value of C_g to the uptake curve onto PE. This adds some uncertainty to the resulting C_g, since concentrations of some PAHs in air likely show short-term fluctuations and diurnal changes.[49–51] Depending on the partition coefficients between air and sampler (or the sampling capacity of the sampler), PE integrates over different time scales for the different compounds[26] (see characteristic times, eqn (1.1)), which additionally varies with season. For instance, lower molecular weight PAHs (*e.g.* Fln) reach chemical equilibrium on PE within hours to days, and the different sampling times could be used to capture short-term variations in air. In contrast, higher molecular weight PAHs, like Fth and Pyr, do not reach equilibrium on PE during the monthly deployment time and C_p integrates over the whole monitoring period. In comparison to the numerical approach (eqn (1.7)), the analytical solution (eqn (1.4)) uses constant values for K_{pg} and D_g over the monitoring period to calculate again an average value for C_g. The resulting C_g varies only slightly from the numerical model, but fluctuations on the PE cannot be captured this way.

Our approach takes no PAH degradation processes into account, as previous tests in the field (sampling with different set-ups, various PRCs and a day *versus* night sampling) confirmed that degradation of PAHs on the sampler is negligible (see ESI†). Many previous studies track loss of PRCs and assume that the loss rate constant of the chosen PRCs equals the uptake rate of target compounds and therefore use several PRCs with a range of physicochemical properties in parallel for kinetics calibration.[13,28,48] Alternatively, sampling rates of the target compounds are calibrated using active and passive samplers simultaneously.[52–56] We compared the air concentrations derived by passive sampling and the numerical model using PRC calibration with concentrations given by active air samplers not for calibration purposes but to test the robustness of the passive sampling approach. The advantage of our approach is that we need only one PRC, as we focus on the air-side boundary layer as the limiting parameter for the exchange of PAHs between air and PE.

3. Results and discussion

3.1. Air-side boundary layers

Fig. 1 shows the measured PRC-loss at each location and the fit to the predicted loss after merging the three sites, which seems valid for the comparable conditions at the study sites. Air-side boundary layer thicknesses (δ_g) determined based on the loss of Ant-D$_{10}$ from PE or the uptake of phenanthrene for each location and for 7 time periods (30 to 36 days each) over 2 years are listed in Table 2 together with the average wind speed, air temperature, global radiation and average K_{pg} during the first three days – the period which was used for calibrating δ_g. Values of δ_g determined from PRC analysis were very similar for the three sites and varied over time likely due to a combination of factors including weather conditions and analytical uncertainties. For instance, in August 2016 and August 2017 almost
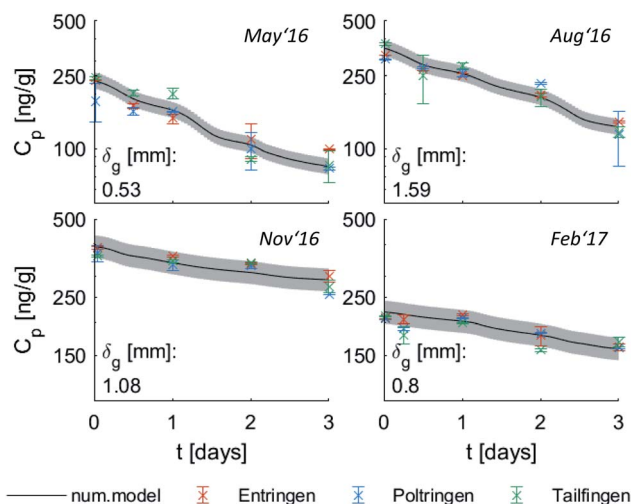
© 2021 The Author(s). Published by the Royal Society of Chemistry

Environ. Sci.: Atmos., 2021, **1**, 253–266 | **257**

Fig. 1 Seasonal PRC-loss during the first year of monitoring, measured at each location and fitted (black solid line) based on measurements averaging over all locations. The air-side boundary layer thickness δ_g was fitted for the average concentrations on PE. Error bars refer to triplicate samples at each location and the grey area indicates the standard deviation of the predicted concentration.

equal wind speeds (2.1 m s^{-1}) and average temperatures (difference less than ~4 °C) were measured at the nearby airport but fitted average values for δ_g differ by a factor of two (1.6 ± 0.34 and 0.80 ± 0.06 mm). Overall, values of δ_g stay in a rather small range with thicknesses between 0.4 mm and 2.3 mm during the two consecutive years and without a seasonal pattern. No obvious correlation could be observed for the thickness of the air-side boundary layer either as a function of air temperature (which varied between −1 °C and 20 °C), wind speed (which was rather stable with 2–3 m s^{-1} during all sampling campaigns) or the solar radiation (which showed higher values during summer). The latter indicates that the sampling design limits photodegradation of PAHs on passive samplers which is a potential issue discussed in literature.[57–59] If photodegradation was causing significant loss of PAHs from PE, we would expect a correlation to solar radiation leading to faster losses of the PRC and thus (artificially) thinner air-side boundary layer in summer, which was not the case. Since Phe

and Ant differ significantly in their photosensitivity,[58–60] the agreement in δ_g calculated using either Ant-D$_{10}$ loss or Phe uptake also indicates that photodegradation of PAHs on PE was not relevant. For a more thorough test on adverse influences on our PAS (like photodegradation), we compared different sampling designs, controlled diurnal variations of PAHs on PE and used Pyr-D$_{10}$ as additional PRC for comparison during some monitorings. None of those tests gave evidence of photodegradation of PAH on PE (see ESI†). Thus, the small range in values of δ_g is likely due to the sampling set-up, with boxes minimizing the influence of wind and solar radiation on the samplers throughout the monitoring periods. This suggests the use of an average value of δ_g independent of the season (here 1 mm) which corresponds to a general calibration of passive sampling kinetics for a specific set-up, such as used before within the Global Atmospheric Passive Sampling network.[7,61] This would then also apply for long-term monitoring of higher molecular weight PAHs which have characteristic time scales for equilibration of several months (Fig. 2). At lower temperatures, characteristic times increase for all compounds due to K_{pg} increasing by up to a factor of ten. Thus, in this case (with rather stable sampling conditions) the exchange between PE and air over seasonal time-scales is more influenced by the physical–chemical properties of the target compounds than by temporal variation of δ_g. Yet, the observed variation of δ_g (±50%) illustrates its uncertainty.

3.2. Uptake of target compounds – comparison of numerical model and analytical solution

Uptake curves of the four PAHs onto PE were fitted both with the numerical model and the analytical solution using the mean δ_g of 1 mm for all sampling campaigns and are shown in Fig. 3. Only the last measurement on PE was used to fit the analytical solution to Fth and Pyr. PE integrates the air concentrations for these two compounds in the linear uptake phase over the entire monitoring campaign, as their long characteristic times indicate. Additionally, higher mass accumulation at the end of the sampling improves certainty in analytical measurement. In contrast, for Fln and Phe all measurements on PE were used to integrate similarly over each time interval during monitoring.

Table 2 Air-side boundary layers (δ_g) in mm, fitted with the numerical model to the loss of Ant-D$_{10}$ from PE sheets during the first three days of each sampling period and for each location individually and average values fitted to the linear uptake of Phe ($\delta_{g,Phe}$) as well as average values of K_{pg}, D_g, temperature (T), wind speed and the sum of the global radiation during the first three days; the overall average of δ_g is 1 mm ± 0.5 mm

| Monitoring	May-16	Aug-16	Nov-16	Feb-17	Aug-17	Nov-17	Feb-18
Entringen $\delta_{g,Ant}$ [mm]	0.5 ± 0.1	1.7 ± 0.1	1.2 ± 0.2	1.2 ± 0.3	0.9 ± 0.1	2.2 ± 0.2	0.8 ± 0.2
Poltringen $\delta_{g,Ant}$ [mm]	0.7 ± 0.1	2.1 ± 0.3	0.9 ± 0.2	1.5 ± 0.2	0.7 ± 0.1	1.3 ± 0.2	0.8 ± 0.1
Tailfingen $\delta_{g,Ant}$ [mm]	0.5 ± 0.1	1.2 ± 0.2	1.4 ± 0.4	1.0 ± 0.3	0.8 ± 0.1	1.4 ± 0.1	0.8 ± 0.2
Avg. $\delta_{g,Ant}$ [mm]	0.6 ± 0.1	1.6 ± 0.3	1.1 ± 0.3	1.4 ± 0.3	0.8 ± 0.1	1.5 ± 0.3	0.8 ± 0.3
Avg. $\delta_{g,Phe}$ [mm]	0.8 ± 0.1	1.3 ± 0.1	1.2 ± 0.2	1.1 ± 0.4	0.9 ± 0.2	1.0 ± 0.1	0.8 ± 0.1
log K_{pg} [L kg^{-1}]	7.78	7.33	8.04	8.12	7.15	7.88	8.26
log D_g [m^2 s^{-1}]	−5.26	−5.24	−5.28	−5.28	−5.23	−5.27	−5.29
T [K]	283.7	292.7	278.8	277	296.45	281.68	275.27
Radiation [J cm^{-2}]	5130	4090	1450	4760	4310	1100	1400
Wind speed [m s^{-1}]	3.1	2.1	1.6	1.3	2.1	1.4	2.7
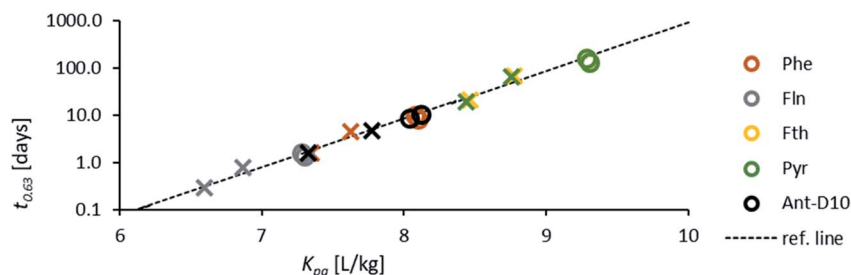
Fig. 2 Characteristic times of fluorene (Fln), phenanthrene (Phe), fluoranthene (Fth) and pyrene (Pyr) to reach 63% of equilibrium on PE for a mean air-side boundary layer thickness δ_g ($=1$ mm) *versus* PE–air partitioning constant K_{pg}; the dotted line covers the range from naphthalene to benzo(*a*)pyrene at a temperature of 20 °C; symbols indicate seasonal sampling values for K_{pg} during autumn and winter (circles) and summer (crosses). Due to their similar properties, Fth and Pyr plot above each other, similar to Phe and Ant during winter.

Fig. 3 shows diurnal and seasonal variations in uptake kinetics of target compounds on PE from air. The seasonal dependency of $t_{0.63}$ is clearly visible with shorter timescales during May and August. In those warmer periods, Fln and Phe reach air-PE equilibrium during the first ~10 days of the sampling campaign. Subsequently, PE concentrations of both compounds fluctuate in response to changing K_{pg} driven by changes in the ambient temperature. This fluctuation is dampened during November and February when characteristic equilibration times are longer. In those colder months, Fth and Pyr demonstrate a linear uptake during the 30-d monitoring periods. Thus, the PE-PAS operate as either equilibrium or kinetic samplers during the deployment of the same duration depending on the compound, and possibly the season.[17] This observation can also be linked directly to the variation of the partition coefficient with temperature driving change in sorption capacity, since the air-side boundary layer (and thus the inherent sampling rate) is not affected by temperature and was observed in our deployments to be as almost constant throughout the year. Significantly higher concentrations on PE were observed during November and February, indicating higher atmospheric concentrations likely due to the increased fuel demand for heating in the winter season (note different scales of C_p in Fig. 3). Both seasonal variations confirm our expectations and support previous studies on PAHs in the atmosphere[62–64] as well as passive sampling kinetics.[61]

Since the numerical model accounts for temperature variation by adapting K_{pg} over time, it is able to capture the fluctuation of the target compounds on the PE, if equilibration is fast. This was clearly observed during February '17 with a decrease of C_p for Fln and Phe induced by an increase of temperature towards the end of the monitoring. The analytical solution, however, averages K_{pg} over the whole sampling period and thus cannot reflect temporal variations on the sampler. By accounting for the temperature variation in K_{pg} throughout each monitoring period, the numerical model can indicate whether a change of concentration on PE is due to a change of temperature alone or in addition to a change in atmospheric concentrations. Large differences between measured and numerically-calculated concentrations on PE indicate a large deviation from average C_g and thus a change of the emission scenario.

3.3. Calculation of average C_g from passive sampling data

To check on the effect of the variation in δ_g for the individual sampling sites and seasons, atmospheric concentrations of the target PAHs were determined both by fitting for each location individually and as an average over the three sites. The outcome for both approaches was in close agreement (Fig. 4(a)) as expected based on the good fit for δ_g (Fig. 1). Only low concentrations (Fth and Pyr) show some deviation from the reference line in excess of a confidence interval of ±30%. The best fit was determined for the more volatile compounds, Fln and Phe, which are already in or close to equilibrium at the end of the sampling campaign (see Fig. 2 for characteristic times). The main deviation was observed for the study site in Entringen with slightly higher concentrations fitted. This site is located close to a railway (diesel fuelled) and is thus likely influenced by this additional emission source. This observation indicates that the uncertainty in data evaluation is rather caused by atmospheric variability than differing air-side boundary layers. The generally good agreement for each site confirmed the reproducibility of the chosen method. Measured concentrations on PE result in 6–9 replicates per sampling time and 72 samples available in total to numerically fit average values of C_g. Fig. 4 compares atmospheric concentrations fitted two ways: (1) using concentrations on PE combined for all locations for the first year of monitoring with seasonal values for δ_g and (2) based on the mean δ_g of 1 mm. As shown in Fig. 4(b) concentrations determined by these two approaches are within a confidence interval of ±30%; although C_g fluctuates significantly throughout the year, the average δ_g is still able to capture those atmospheric variations.

Similarly, atmospheric concentrations determined with the numerical model and the analytical solution applying a constant air-side boundary layer of 1 mm agreed reasonably well (Fig. S8†). Only for Pyr some clear deviations could be observed during the warmer periods when atmospheric concentrations of Pyr as well as the concentrations on the sampler are very low. This is already visible for the uptake onto the sampler in Fig. 3 with unexpectedly high concentrations in the beginning, followed by a decrease towards the end of the monitoring. Hence, the numerical model, which accounts for all sampling times, leads to a higher concentration in air than
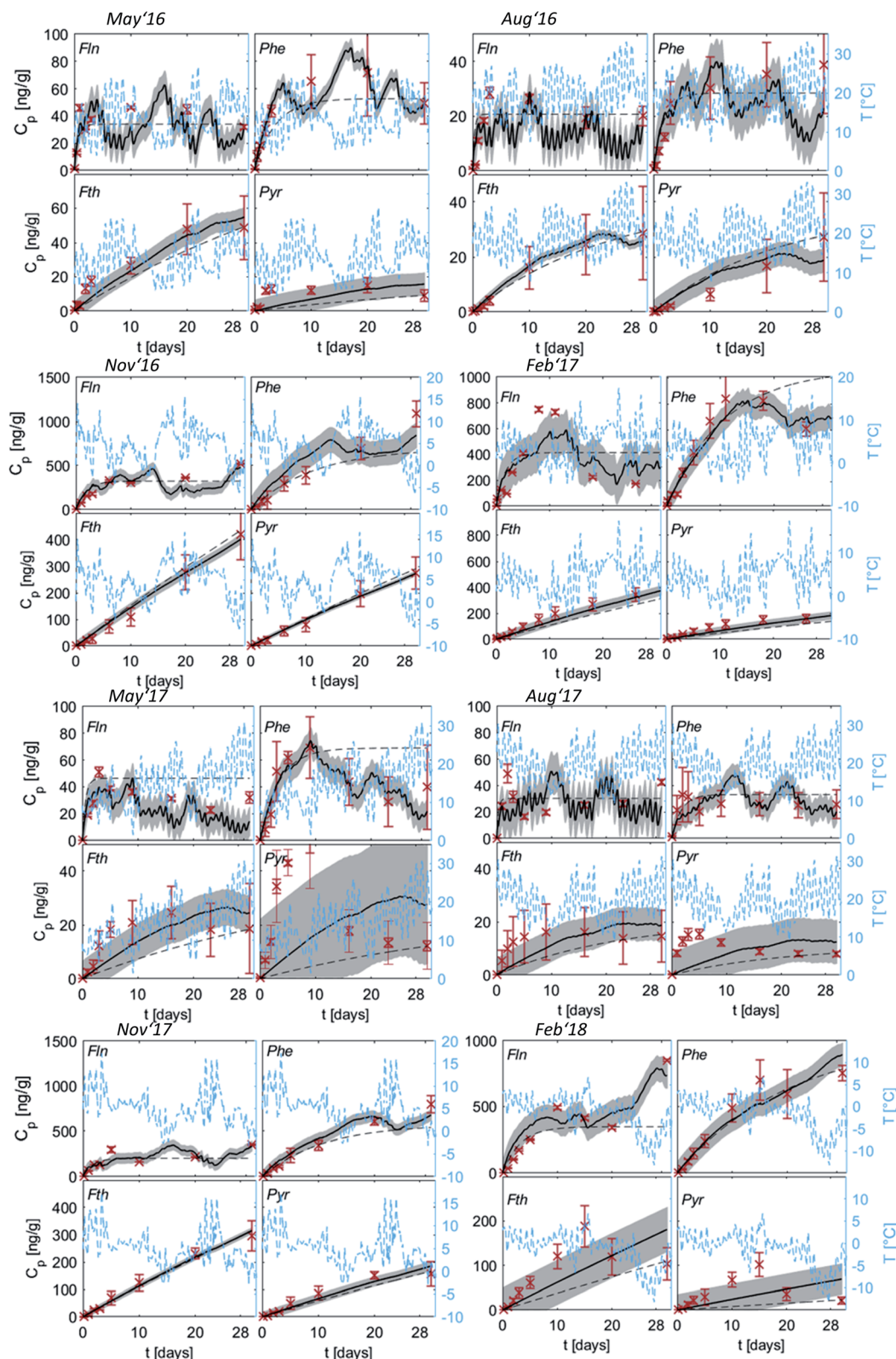
© 2021 The Author(s). Published by the Royal Society of Chemistry

Environ. Sci.: Atmos., 2021, **1**, 253–266 | **259**

Fig. 3 Measured (red crosses) and modelled uptake curves of the four representative PAHs (averaged for all three sites) along with the temperature changes (blue); grey areas indicate standard deviations calculated with the numerical model (solid line), error bars refer to the standard deviation of the measured replicates, dashed lines indicate the analytical solution (exponential function, eqn (1.4)). For a better illustration of low values, concentrations of Fln and Pyr are multiplied with a factor of five. For Fln this is done for all seasons, while for Pyr this was necessary only during May and August 2017.
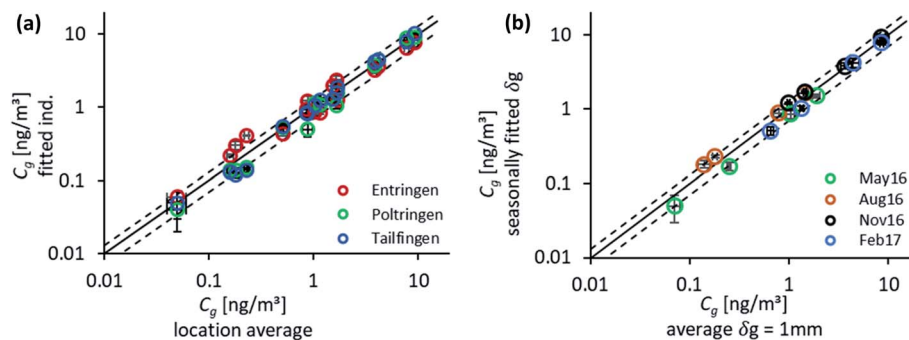
Fig. 4 Scatter plots of fitted atmospheric concentrations (numerical model) of the four target PAHs for (a) C_g fitted for each location individually *versus* C_g averaging over the three sites and (b) combining the three sites with C_g based on a seasonal δ_g *versus* the average δ_g of 1 mm. A reference line (1 : 1) as well as a 30% confidence interval is included, and the error bars of the measurement refer to the standard deviation calculated for the numerical model.

the analytical solution which is based only on the last sampling point.

Earlier studies have illustrated how complex the determination of precise sampling rates is and how easily errors can be made when calibrating passive samplers.[7,65] Sampling rates, or the amount of target compound sampled usually expressed as air volume per time,[66–68] for a given PAS configuration are reported to vary over several orders of magnitude, depending on the environmental conditions, the considered time span, the target compound, and even the concentrations on the passive samplers.[15,56,69,70] Since they are significantly influenced by the ambient temperature, wind speed and wind angle, sampling rates can vary considerably within a sampling campaign. The air-side boundary layer would be influenced by ambient conditions like wind speed and wind angle in the same way as the inherent sampling rate. In the present field study, we observed a good reproducibility of this parameter due to the similarity of sites and conditions. Thus, for stable sampling conditions the general calibration of PE-passive samplers using δ_g seems justified, as for sampling rate. Yet, an ease and transparency of comparison is provided by using δ_g as it does not change with the surface area of the sampler, nor for the target compounds.

3.4. Comparison of C_g from passive to active sampling

Active sampling was conducted at one location (Entringen) in November 2017 and February 2018 to reference against air concentrations determined by PE-PAS. Active samplers filtered about 4 m^3 of air during 3–5 days, sampling periodically for 16 hours with intervals (of up to 8 hours) to recharge the batteries. For both monitorings we sampled two time-spans to check on short-term variations of C_g. During November the respective time-spans were 18.11.17 to 22.11.17 and 1.12.17 to 4.12.17, and during February the time-spans were 15.2.18 to 20.2.18 and 25.2.18 to 28.2.18. LMW PAHs (Fln, Phe) are expected to have reached equilibrium state on PE at this point and thus are better suited for comparison. As listed in Table 3, significant variation of C_g during this cold period was only observed for Fth and Pyr with a decrease of C_g for a factor of ten towards the last sampling period (25. to 28.2.18). Although PAHs were below

quantification limit on the glass fibre filters, the influence of particles on C_g determined on active samplers (PUF filters) cannot be completely excluded as shown in earlier studies,[70] where Phe, Fth and Pyr sorbed to ultrafine particles under 100 nm (smaller than the pore size of the glass fibre filters) were found on PUF filters. As no PAHs were detected on glass fibre filters during the second sampling in February 2018, perhaps this indicates that particulates in air were at a lower level and therefore leading to a lower contribution of particle influence on PUF. Due to the strong sorption of Fth and Pyr to particles, a small amount of (accidentally) sampled particles could cause a significant measurement bias on the resulting atmospheric concentrations.[56,70]

Fig. 5 compares results from passive samplers (evaluated with the numerical model) and C_g measured with active samplers during November 2017 (18.11.17 to 22.11.17) and February 2018 (15.2.18 to 20.2.18). A very good agreement was obtained for Fln and Phe during both monitoring periods. For Fth and Pyr, a reasonable agreement within the range of uncertainty can be observed for November, while during February the active samplers provide higher atmospheric concentrations than determined with passive samplers. This can be due to the different time spans, and thus different air masses, which are reflected by the two methods. A direct comparison of C_g based on different sampling methods can only be valid if the same air masses are sampled, otherwise the different methods can be influenced by varying atmospheric concentrations.[53,56] In our study, due to the short 3–5 days duration of the active sampling, active and passive samplers integrate only for Fln over the same time span and reflect the

Table 3 Atmospheric concentrations [ng m^{-3}] of Fln, Phe, Fth and Pyr determined with active samplers covering two individual time spans in November 2017/December 2017 and February 2018

Monitoring	Fln	Phe	Fth	Pyr
Active: 18.11. to 22.11.17	2.8 ± 0.3	9.0 ± 4.3	2.2 ± 0.1	1.4 ± 0.1
Active: 1.12. to 4.12.17	3.3 ± 0.1	13.0 ± 0.1	2.1 ± 0.1	1.7 ± 0.1
Active: 15.2. to 20.2.18	2.6 ± 0.8	8.9 ± 0.9	2.1 ± 0.2	1.0 ± 0.2
Active: 25.2. to 28.2.18	0.9 ± 0.4	12.5 ± 2.9	0.2 ± 0.1	0.1 ± 0.1

© 2021 The Author(s). Published by the Royal Society of Chemistry

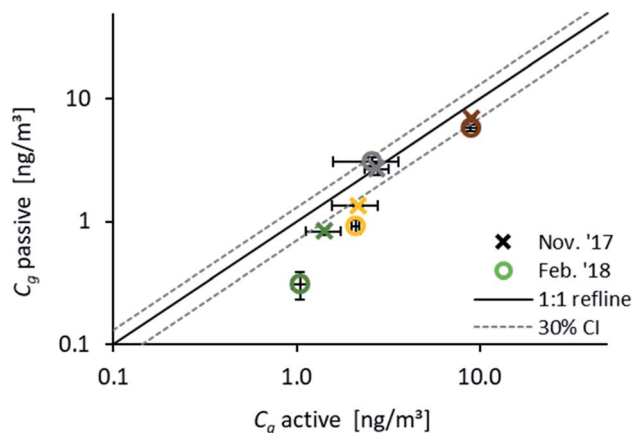*Environ. Sci.: Atmos.*, 2021, **1**, 253–266 | **261**

Fig. 5 log–log scatter plot of atmospheric concentrations of Fln (grey), Phe (brown), Fth (yellow) and Pyr (green) determined with passive samplers in deployments over 3-November to 3-December and 1–15 February using the numerical model based on the seasonal δ_g (1.6 mm) *versus* concentrations measured with active samplers in deployments over 18–22 November 2017 and 15–20 February 2018 in Entringen. Error bars show the standard deviation of the triplicate samples (passive and active).

same concentration in air. This is the same observation as reported by Melymuk *et al.*[15] Again, the calculated t_{63} can be used to identify the compound-specific time span to reach 63% equilibration by the passive sampler. With a t_{63} on the order of days (Fig. 1), Fln is the most reliable of the chosen PAHs for a comparison of those two sampling methods. An average ratio of one for $C_{g,active}/C_{g,passive}$ for Fln confirms the presented passive sampling approach as a valid method to measure gaseous concentrations of PAHs.

3.5. The use of characteristic ratios

Fig. 6 shows the distribution pattern of the four PAHs in air during each of the seasonal sampling campaigns between May 2016 and February 2018. Concentrations included within

Fig. 6(a) were fitted with the numerical model to the respective uptake curves on the PE. As described above, the three study sites were combined as they reflect the same geographic area with only slight concentration differences. Therefore, up to nine replicates were considered per sampling time (and 72 samples per fitting routine), resulting in robust average values, particularly with respect to the observed pattern. Fig. 6(a) illustrates two characteristic features: (i) atmospheric concentrations are higher in the heating period during autumn and winter during both years (confirming the observation of Fig. 3) and (ii) Phe has the highest concentrations in air throughout the whole monitoring period, followed by Fln, while Fth and Pyr show only low atmospheric concentrations. The remainder of the 16 U.S. EPA priority PAHs targeted in the analytical method have lower concentrations than these four, except for naphthalene, which is in the same range as Fln. Fig. 6(b) demonstrates the very good reproducibility of this characteristic distribution pattern throughout all sampling campaigns. This also holds for active samplers, except for the second campaign in February (Fig. S9†), which may be explained by a lower influence of particles on PUF filters during this period. Stable characteristic distribution patterns allow the calculation of concentrations of several compounds based on just a few or one reference compound, *e.g.* Phe. This approach was presented for soils by Wilcke[71] and Bucheli *et al.*,[72] who determined very stable distribution patterns of PAHs in a broad range of soils and used specific ratios to calculate concentrations of several PAHs based on the measurement of one reference PAH. Earlier studies on PAH atmospheric deposition in southwestern Germany also report very consistent distribution patterns with highest amounts for Phe.[73,74]

Based on these findings, Phe may be applied as a reference to calculate the concentrations of other PAHs within soil or the atmosphere. Phenanthrene was chosen as a reference compound, as we observed highest concentrations and lowest standard deviation for replicate samples. For this approach, the
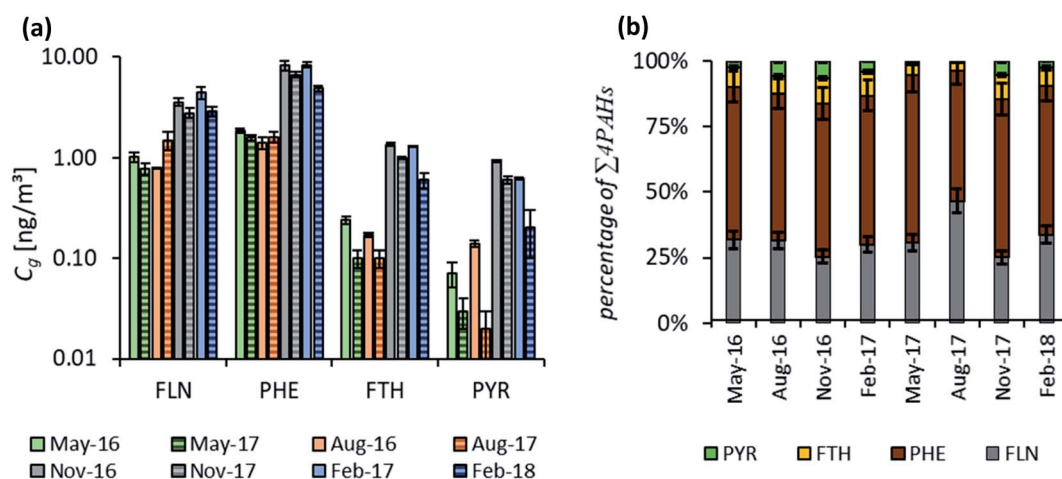

Fig. 6 (a) Atmospheric concentrations of the four representative PAHs determined by passive sampling averaged over all sites. Error bars indicate standard deviation of 9 replicates. (b) Distribution pattern of the four representative PAHs, error bars for FLN and PHE are set to a standard deviation of 10%.
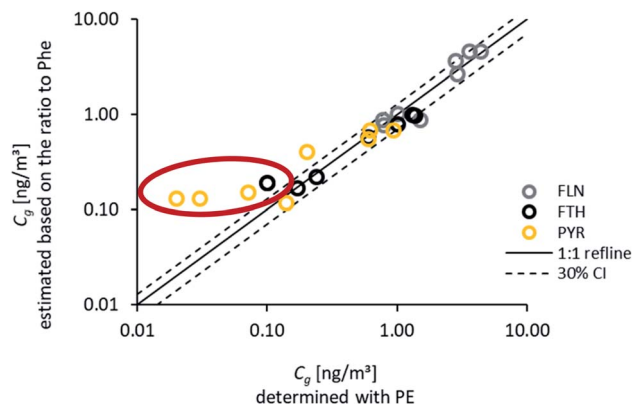
Fig. 7 Atmospheric concentrations of Fln, Fth and Pyr for all seasons and all locations calculated from Phe and the average distribution pattern during August 2016. The red circle denotes outliers of Pyr during the warm periods as well as Fth during August 2017.

ratios of Fln/Phe, Fth/Phe and Pyr/Phe were calculated for C_g during summer 2016. Subsequently, those ratios were used in combination with the fitted C_g of Phe during all other monitoring periods to estimate C_g for Fln, Fth and Pyr. A very good agreement, with the majority within ±30%, was obtained for all atmospheric concentrations above 0.1 ng m^{-3} (Fig. 7). As discussed above, lower concentrations near analytical detection limits are more uncertain, and this issue is most pronounced for Pyr during the warmest sampling campaigns. This results in distinctively higher concentrations of Pyr estimated than those fitted with the numerical model (marked in the figure). For unknown reasons, the observed uptake of Pyr onto PE is considerably faster than calculated with the numerical model (Fig. 3) except for August 2016, which might lead to an underestimation of the corresponding C_g. Using an average ratio of Pyr/Phe to account for all sampling campaigns with $C_g > 0.1$ ng m^{-3} leads to slightly lower atmospheric concentrations (factor 0.8) than the specific ratio during summer 2016. For Fln and Fth no difference was observed for an average ratio (Fig. S10†). Interestingly, Melymuk et al.[15] also observed unexpectedly high passive sampling rates during the first half of the year for Fth and Pyr. However, the generally good agreement of estimated and fitted concentrations can be accepted to confirm the reliability of this approach to use one reference compound and stable ratios to determine the whole range of atmospheric concentrations. This allows to overcome exceedingly long monitoring times otherwise required for high molecular weight PAHs on the passive samplers and can be used to reduce the uncertainty caused by the measurement of very low concentrations. Yet, it should be noted, that such an approach is only valid in certain areas for which homogenously mixed air masses or stable distribution patterns have been observed.

4. Conclusions

As the uptake kinetics of passive samplers in the atmosphere vary significantly for the different compounds and seasons, the characteristic times to 63% equilibration ($t_{0.63}$) provide a useful

and convenient measure of the time span over which PAS integrate individual target compounds. Knowledge of the characteristic times helps to improve the planning of sampling campaigns as well as the evaluation of measured concentrations. Providing a consistent design for the passive samplers in the field allows the use of one (average) air-side boundary layer for the data evaluation, which is specific for the sampling set-up, but according to our results is (almost) independent of location and season. Thus, a set-up specific value may be taken (here 1 mm) for all compounds. Numerical modelling shows that even diurnal temperature changes affect the loading of the passive samplers for compounds with log $K_{pg} < 8$ L kg^{-1} because of the temperature sensitivity of partition coefficients. Hence, combining measured uptake curves (time series) with such a modelling approach allows for the identification of (short-term) concentration changes in the atmosphere. C_g probably fluctuates rapidly (diurnal) and significantly for many SVOCs of interest for passive air sampling and if the goal is to get average concentrations then for compounds with fast equilibration with PE-PAS (Fln, Phe) several measurements are needed during the considered time span. Compounds with log $K_{pg} > 9$ L kg^{-1} only reach equilibrium after long time periods (at least 100 days) and yield a stable average during the linear uptake period for shorter deployments (in principle just one data point is needed), but for these compounds the uptake is very low and often below the limit of quantification. One way to solve this dilemma would be focusing on a representative PAH covering the desired monitoring time span and using PAH ratios to calculate other compounds of interest. Based on the present study a good candidate could be Phe, which shows the highest concentrations in air and on the sampler and thus the lowest uncertainty for the data-evaluation.

Conflicts of interest

There are no conflicts to declare.

Acknowledgements

References

1 C. J. Halsall, et al., Spatial and Temporal Variation of Polycyclic Aromatic Hydrocarbons in the Arctic Atmosphere, Environ. Sci. Technol., 1997, **31**(12), 3593–3599.

2 A. Cabrerizo, et al., Climatic and biogeochemical controls on the remobilization and reservoirs of persistent organic pollutants in Antarctica, Environ. Sci. Technol., 2013, **47**(9), 4299–4306.

3 S. M. Bengtson Nash, et al., Persistent Organic Pollutants in the East Antarctic Atmosphere: Inter-Annual Observations

© 2021 The Author(s). Published by the Royal Society of Chemistry

Environ. Sci.: Atmos., 2021, **1**, 253–266 | **263**

from 2010 to 2015 Using High-Flow-Through Passive Sampling, *Environ. Sci. Technol.*, 2017, **51**(23), 13929–13937.

4 L. Tuduri, *et al.*, Passive air sampling of semi-volatile organic compounds, *TrAC, Trends Anal. Chem.*, 2012, **31**, 38–49.

5 B. Vrana, *et al.*, Passive sampling techniques for monitoring pollutants in water, *TrAC, Trends Anal. Chem.*, 2005, **24**(10), 845–868.

6 A. Kot-Wasik, *et al.*, Advances in passive sampling in environmental studies, *Anal. Chim. Acta*, 2007, **602**(2), 141–163.

7 F. Wania and C. Shunthirasingham, Passive air sampling for semi-volatile organic chemicals, *Environ. Sci.: Processes Impacts*, 2020, **22**(10), 1925–2002.

8 A. Sobek, *et al.*, Coastal sediments in the Gulf of Bothnia as a source of dissolved PCDD/Fs and PCBs to water and fish, *Sci. Total Environ.*, 2014, **487**, 463–470.

9 N. C. Niehus, B. Brockmeyer and G. Witt, Bioavailability and distribution of PAHs and PCBs in the sediment pore water of the German Bight and Wadden Sea, *Mar. Pollut. Bull.*, 2019, **138**, 421–427.

10 B. Beckingham and U. Ghosh, Polyoxymethylene passive samplers to monitor changes in bioavailability and flux of PCBs after activated carbon amendment to sediment in the field, *Chemosphere*, 2013, **91**(10), 1401–1407.

11 Y. Liu, *et al.*, Gaseous and Freely-Dissolved PCBs in the Lower Great Lakes Based on Passive Sampling: Spatial Trends and Air–Water Exchange, *Environ. Sci. Technol.*, 2016, **50**(10), 4932–4939.

12 R. Lohmann, *et al.*, Determining air–water exchange, spatial and temporal trends of freely dissolved PAHs in an urban estuary using passive polyethylene samplers, *Environ. Sci. Technol.*, 2011, **45**(7), 2655–2662.

13 E. J. Morgan and R. Lohmann, Detecting air–water and surface-deep water gradients of PCBs using polyethylene passive samplers, *Environ. Sci. Technol.*, 2008, **42**(19), 7248–7253.

14 B. Zabiegała, *et al.*, Passive sampling as a tool for obtaining reliable analytical information in environmental quality monitoring, *Anal. Bioanal. Chem.*, 2010, **396**(1), 273–296.

15 L. Melymuk, *et al.*, Evaluation of passive air sampler calibrations: Selection of sampling rates and implications for the measurement of persistent organic pollutants in air, *Atmos. Environ.*, 2011, **45**(10), 1867–1875.

16 L. A. Schifman and T. B. Boving, Spatial and seasonal atmospheric PAH deposition patterns and sources in Rhode Island, *Atmos. Environ.*, 2015, **120**, 253–261.

17 T. Harner, *et al.*, Passive air sampling for persistent organic pollutants: introductory remarks to the special issue, *Environ. Pollut.*, 2006, **144**(2), 361–364.

18 J. N. Huckins, *et al.*, Lipid-containing semipermeable membrane devices for monitoring organic contaminants in water, *Environ. Sci. Technol.*, 1993, **27**(12), 2489–2496.

19 M. Shoeib and T. Harner, Characterization and Comparison of Three Passive Air Samplers Persistent Organic Pollutants, *Environ. Sci. Technol.*, 2002, **36**(19), 4142–4151.

20 M. E. Bartkow, *et al.*, Characterizing Uptake Kinetics of PAHs from the Air Using Polyethylene-Based Passive Air Samplers of Multiple Surface Area-to-Volume Ratios, *Environ. Sci. Technol.*, 2004, **38**(9), 2701–2706.

21 M. E. Bartkow, *et al.*, Passive air sampling theory for semivolatile organic compounds, *Chemosphere*, 2005, **60**(2), 170–176.

22 M. A. Khairy and R. Lohmann, Field validation of polyethylene passive air samplers for parent and alkylated PAHs in Alexandria, Egypt, *Environ. Sci. Technol.*, 2012, **46**(7), 3990–3998.

23 W. G. Whitman, The two film theory of gas absorption, *Int. J. Heat Mass Transfer*, 1962, **5**(5), 429–433.

24 K. Pozo, *et al.*, Seasonally Resolved Concentrations of Persistent Organic Pollutants in the Global Atmosphere from the First Year of the GAPS Study, *Environ. Sci. Technol.*, 2009, **43**(3), 796–803.

25 P. Mayer, *et al.*, Equilibrium sampling devices, *Environ. Sci. Technol.*, 2003, **37**(9), 184A–191A.

26 T. Harner, *et al.*, Passive air sampling for persistent organic pollutants: Introductory remarks to the special issue, *Environ. Pollut.*, 2006, **144**(2), 361–364.

27 C. Moeckel, *et al.*, Use of Depuration Compounds in Passive Air Samplers: Results from Active Sampling-Supported Field Deployment, Potential Uses, and Recommendations, *Environ. Sci. Technol.*, 2009, **43**(9), 3227–3232.

28 H. S. Söderström and P.-A. Bergqvist, Passive Air Sampling Using Semipermeable Membrane Devices at Different Wind-Speeds *in Situ* Calibrated by Performance Reference Compounds, *Environ. Sci. Technol.*, 2004, **38**(18), 4828–4834.

29 W. A. Ockenden, F. M. Jaward and K. C. Jones, Atmospheric sampling of persistent organic pollutants: needs, applications and advances in passive air sampling techniques, *Sci. World J.*, 2001, **1**, 557–575.

30 L. Tuduri, T. Harner and H. Hung, Polyurethane foam (PUF) disks passive air samplers: Wind effect on sampling rates, *Environ. Pollut.*, 2006, **144**(2), 377–383.

31 M. E. Bartkow, *et al.*, Evaluation of performance reference compounds in polyethylene-based passive air samplers, *Environ. Pollut.*, 2006, **144**(2), 365–370.

32 J. N. Huckins, *et al.*, Determination of Uptake Kinetics (Sampling Rates) by Lipid-Containing Semipermeable Membrane Devices (SPMDs) for Polycyclic Aromatic Hydrocarbons (PAHs) in Water, *Environ. Sci. Technol.*, 1999, **33**(21), 3918–3923.

33 R. D. Wijayaratne and J. C. Means, Sorption of Polycyclic aromatic hydrocarbons by natural estuarine colloids, *Mar. Environ. Res.*, 1984, **11**(2), 77–89.

34 K. C. Jones, *et al.*, Organic contaminants in Welsh soils: polynuclear aromatic hydrocarbons, *Environ. Sci. Technol.*, 1989, **23**(5), 540–550.

35 M. Howsam and K. C. Jones, Sources of PAHs in the Environment, in *PAHs and Related Compounds: Chemistry*, ed. A. H. Neilson, Springer Berlin Heidelberg, Berlin, Heidelberg, 1998, pp. 137–174.

36 M. V. Roux, *et al.*, Critically Evaluated Thermochemical Properties of Polycyclic Aromatic Hydrocarbons, *J. Phys. Chem. Ref. Data*, 2008, **37**(4), 1855.

37 K. C. Jones, Observations on long-term air–soil exchange of organic contaminants, *Environ. Sci. Pollut. Res.*, 1994, **1**(3), 172.

38 Y. Dumanoglu, *et al.*, Spatial and seasonal variations, sources, air–soil exchange, and carcinogenic risk assessment for PAHs and PCBs in air and soil of Kutahya, Turkey, the province of thermal power plants, *Sci. Total Environ.*, 2017, **580**, 920–935.

39 E. Kaya, *et al.*, Spatial and temporal variation and air–soil exchange of atmospheric PAHs and PCBs in an industrial region, *Atmos. Pollut. Res.*, 2012, **3**(4), 435–449.

40 Z. Wu, *et al.*, Air–sea exchange and gas–particle partitioning of polycyclic aromatic hydrocarbons over the northwestern Pacific Ocean: Role of East Asian continental outflow, *Environ. Pollut.*, 2017, **230**, 444–452.

41 I. J. Allan, *et al.*, Effect of sampler material on the uptake of PAHs into passive sampling devices, *Chemosphere*, 2010, **79**(4), 470–475.

42 R. Lohmann, Critical review of low-density polyethylene's partitioning and diffusion coefficients for trace organic contaminants and implications for its use as a passive sampler, *Environ. Sci. Technol.*, 2012, **46**(2), 606–618.

43 K. E. Kennedy, *et al.*, A field comparison of ethylene vinyl acetate and low-density polyethylene thin films for equilibrium phase passive air sampling of polycyclic aromatic hydrocarbons, *Atmos. Environ.*, 2007, **41**(27), 5778–5787.

44 K. Booij, S. Foppe and E. M. van Weerlee, Spiking of performance reference compounds in low density polyethylene and silicone passive water samplers, *Chemosphere*, 2002, **46**, 1157–1161.

45 J. N. Huckins, *et al.*, Development of the Permeability/Performance Reference Compound Approach for *In Situ* Calibration of Semipermeable Membrane Devices, *Environ. Sci. Technol.*, 2002, **36**(1), 85–91.

46 T. Harner, *et al.*, Characterization of Polymer-Coated Glass as a Passive Air Sampler for Persistent Organic Pollutants, *Environ. Sci. Technol.*, 2003, **37**(11), 2486–2493.

47 Y.-G. Ma, *et al.*, Critical Review and Recommended Values for the Physical–Chemical Property Data of 15 Polycyclic Aromatic Hydrocarbons at 25 °C, *J. Chem. Eng. Data*, 2010, **55**(2), 819–825.

48 M. A. Khairy and R. Lohmann, Field calibration of low density polyethylene passive samplers for gaseous POPs, *Environ. Sci.: Processes Impacts*, 2014, **16**(3), 414–421.

49 Z. Bao, *et al.*, Modeling short-term concentration fluctuations of semi-volatile pollutants in the soil–plant–atmosphere system, *Sci. Total Environ.*, 2016, **569–570**, 159–167.

50 R. G. M. Lee, *et al.*, Measurement and Modeling of the Diurnal Cycling of Atmospheric PCBs and PAHs, *Environ. Sci. Technol.*, 1998, **32**(14), 2172–2179.

51 J. Liu, *et al.*, Diurnal and nocturnal variations of PAHs in the Lhasa atmosphere, Tibetan Plateau: Implication for local sources and the impact of atmospheric degradation processing, *Atmos. Res.*, 2013, **124**, 34–43.

52 S. J. Hayward, T. Gouin and F. Wania, Comparison of Four Active and Passive Sampling Techniques for Pesticides in Air, *Environ. Sci. Technol.*, 2010, **44**(9), 3410–3416.

53 T. Gouin, *et al.*, Passive and Active Air Samplers as Complementary Methods for Investigating Persistent Organic Pollutants in the Great Lakes Basin, *Environ. Sci. Technol.*, 2005, **39**(23), 9115–9122.

54 J. M. Armitage, S. J. Hayward and F. Wania, Modeling the Uptake of Neutral Organic Chemicals on XAD Passive Air Samplers under Variable Temperatures, External Wind Speeds and Ambient Air Concentrations (PAS-SIM), *Environ. Sci. Technol.*, 2013, **47**(23), 13546–13554.

55 C. Chaemfa, *et al.*, Field calibration of polyurethane foam (PUF) disk passive air samplers for PCBs and OC pesticides, *Environ. Pollut.*, 2008, **156**(3), 1290–1297.

56 K. M. Ellickson, *et al.*, Analysis of polycyclic aromatic hydrocarbons (PAHs) in air using passive sampling calibrated with active measurements, *Environ. Pollut.*, 2017, **231**, 487–496.

57 I. J. Allan, *et al.*, Photodegradation of PAHs in passive water samplers, *Mar. Pollut. Bull.*, 2016, **105**(1), 249–254.

58 M. E. Bartkow, *et al.*, Photodegradation of polyaromatic hydrocarbons in passive air samplers: field testing different deployment chambers, *Environ. Pollut.*, 2006, **144**(2), 371–376.

59 T. D. Behymer and R. A. Hites, Photolysis of polycyclic aromatic hydrocarbons adsorbed on simulated atmospheric particulates, *Environ. Sci. Technol.*, 1985, **19**(10), 1004–1006.

60 W. W. Brubaker and R. A. Hites, OH Reaction Kinetics of Polycyclic Aromatic Hydrocarbons and Polychlorinated Dibenzo-*p*-dioxins and Dibenzofurans, *J. Phys. Chem. A*, 1998, **102**(6), 915–921.

61 J. Klánová, *et al.*, Assessing the Influence of Meteorological Parameters on the Performance of Polyurethane Foam-Based Passive Air Samplers, *Environ. Sci. Technol.*, 2008, **42**(2), 550–555.

62 K. Prevedouros, *et al.*, Seasonal and long-term trends in atmospheric PAH concentrations: evidence and implications, *Environ. Pollut.*, 2004, **128**(1), 17–27.

63 J. Masih, *et al.*, Seasonal Variation and Sources of Polycyclic Aromatic Hydrocarbons (PAHs) in Indoor and Outdoor Air in a Semi Arid Tract of Northern India, *Aerosol Air Qual. Res.*, 2012, **12**(4), 515–525.

64 L.-Y. Liu, *et al.*, Differences in spatiotemporal variations of atmospheric PAH levels between North America and Europe: Data from two air monitoring projects, *Environ. Int.*, 2014, **64**, 48–55.

65 S. Hazrati and S. Harrad, Calibration of polyurethane foam (PUF) disk passive air samplers for quantitative measurement of polychlorinated biphenyls (PCBs) and polybrominated diphenyl ethers (PBDEs): Factors influencing sampling rates, *Chemosphere*, 2007, **67**(3), 448–455.

66 K. Pozo, *et al.*, Toward a Global Network for Persistent Organic Pollutants in Air: Results from the GAPS Study, *Environ. Sci. Technol.*, 2006, **40**(16), 4867–4873.

© 2021 The Author(s). Published by the Royal Society of Chemistry

Environ. Sci.: Atmos., 2021, **1**, 253–266 | **265**

67 L. B. Paulik, *et al.*, Emissions of Polycyclic Aromatic Hydrocarbons from Natural Gas Extraction into Air, *Environ. Sci. Technol.*, 2016, **50**(14), 7921–7929.

68 N. J. Herkert, *et al.*, Calibration and evaluation of PUF-PAS sampling rates across the Global Atmospheric Passive Sampling (GAPS) network, *Environ. Sci.: Processes Impacts*, 2018, **20**(1), 210–219.

69 C. Persoon and K. C. Hornbuckle, Calculation of passive sampling rates from both native PCBs and depuration compounds in indoor and outdoor environments, *Chemosphere*, 2009, **74**(7), 917–923.

70 P. Bohlin, *et al.*, Outdoor passive air monitoring of semi volatile organic compounds (SVOCs): a critical evaluation of performance and limitations of polyurethane foam (PUF) disks, *Environ. Sci.: Processes Impacts*, 2014, **16**(3), 433–444.

71 W. Wilcke, Synopsis Polycyclic Aromatic Hydrocarbons (PAHs) in Soil—a Review, *J. Plant Nutr. Soil Sci.*, 2000, **163**(3), 229–248.

72 T. D. Bucheli, *et al.*, Polycyclic aromatic hydrocarbons, black carbon, and molecular markers in soils of Switzerland, *Chemosphere*, 2004, **56**(11), 1061–1076.

73 T. Gocht, *et al.*, Indications for pedogenic formation of perylene in a terrestrial soil profile: Depth distribution and first results from stable carbon isotope ratios, *Appl. Geochem.*, 2007, **22**(12), 2652–2663.

74 T. Gocht, O. Klemm and P. Grathwohl, Long-term atmospheric bulk deposition of polycyclic aromatic hydrocarbons (PAHs) in rural areas of Southern Germany, *Atmos. Environ.*, 2007, **41**(6), 1315–1327.

© 2021 The Author(s). Published by the Royal Society of Chemistry